JOURNAL OF GEOPHYSICAL RESEARCH, VOL. 114, D09211, doi:10.1029/2008JD011273, 2009

Global observations of aerosol impacts on precipitation occurrence in warm maritime clouds

Tristan S. L'Ecuyer,[1] Wesley Berg,[1] John Haynes,[1] Matthew Lebsock,[1] and Toshihiko Takemura[2]

Received 9 October 2008; revised 16 January 2009; accepted 19 March 2009; published 8 May 2009.

[1] The impact of aerosols on precipitation occurrence in warm clouds is assessed using a combination of multisensor satellite cloud and precipitation data sets and aerosol information from both satellite and a global transport model. Aerosols are found to suppress the formation of precipitation in polluted regions, evidenced by a trend toward higher liquid water path prior to the onset of light rainfall. Polluted clouds are also found to be more vertically developed than those in more pristine environments. Coupled with an apparent reduction in the size of the raindrops that subsequently form in these clouds, these findings indicate that pollution inhibits precipitation processes by redistributing water among a greater number of smaller cloud droplets. Evidence is also provided that sea-salt aerosols have the opposite effect on precipitation development. Maritime clouds that form in regions of enhanced sea-salt concentrations tend to precipitate more frequently, form larger raindrops, and be less vertically developed. This suggests that the nucleation of sea-salt particles may provide a source of embryonic raindrops in maritime clouds accelerating precipitation processes and ultimately reducing cloud lifetime. The net effect of aerosols on the onset of precipitation in any given region is, therefore, defined by the relative magnitudes of the competing effects of sulfate aerosols and sea-salt particles, the strengths of which depend strongly on both cloud liquid water path and the thermodynamic properties of the local environment.

Citation: L'Ecuyer, T. S., W. Berg, J. Haynes, M. Lebsock, and T. Takemura (2009), Global observations of aerosol impacts on precipitation occurrence in warm maritime clouds, *J. Geophys. Res.*, *114*, D09211, doi:10.1029/2008JD011273.

1. Introduction

[2] Recent satellite estimates suggest that clouds account for 40% of the global albedo and reduce the amount of thermal radiation emitted to space by 10% relative to clear-sky conditions [*L'Ecuyer et al.*, 2008]. Small changes in cloud albedo, their vertical distribution, and their lifetimes can, therefore, have a significant impact on the distribution of radiative heating around the globe. Since the early observations of differences between continental and maritime clouds by *Squires* [1956, 1958], variations in the concentration of aerosols have been recognized as a potential pathway for large-scale modification of the microphysical properties of clouds. *Twomey* [1977] and *Twomey et al.* [1984] proposed that, for a for a fixed liquid water path (LWP), increases in the concentration of cloud condensation nuclei (CCN) resulting from anthropogenic aerosols should cause liquid clouds to become brighter and optically thicker. *Albrecht* [1989] suggested that this effect may be further enhanced by a second aerosol indirect effect where increased concentrations of CCN may inhibit coalescence processes in warm clouds thereby suppressing the formation of precipitation and increasing cloud lifetime and, thus, fractional cloud cover. The combination of increased albedo and longer-lived clouds could impart a significant cooling to partially offset the warming effects of increased greenhouse gas concentrations in the Earth's atmosphere.

[3] The impacts of enhanced aerosol concentrations on cloud effective radius have been explored using both regional and global satellite data sets [e.g., *Nakajima et al.*, 2001; *Bréon et al.*, 2002; *Feingold et al.*, 2003; *Matsui et al.*, 2006; *Lebsock et al.*, 2008] and the results have been applied to estimate the magnitude of the cloud albedo effect using climate models [e.g., *Rotstayn and Liu*, 1999; *Ghan et al.*, 2001; *Jones et al.*, 2001; *Lohmann and Feichter*, 2001; *Forster et al.*, 2007, and references therein]. A number of modeling studies have also provided evidence for the suppression of precipitation in areas of high aerosol loading [e.g., *Jiang et al.*, 2002; *Lu and Seinfeld*, 2005; *Jacobson et al.*, 2007] but, to date, much of the observational evidence for the second indirect effect comes from regional studies. *Rosenfeld* [2000] and *Givati and Rosenfeld* [2004], for example, identified several scenes where cloud drop size is reduced and precipitation suppressed as a result of industrial and urban air pollution while others have shown that the concentrations of drizzle drops in marine stratocu-

[1]Department of Atmospheric Science, Colorado State University, Fort Collins, Colorado, USA.
[2]Research Institute for Applied Mechanics, Kyushu University, Fukuoka, Japan.

0148-0227/09/2008JD011273$09.00

mulus tend to be reduced in ship tracks [e.g., *Ferek et al.*, 2000]. Global evidence for increased cloud lifetime and precipitation suppression by aerosols has been more elusive, in part because of the challenges associated with precise delineation of the transition from cloud to precipitation using conventional satellite instrumentation. The results of the study of *Sekiguchi et al.* [2003] suggest that cloud fraction may be correlated with aerosol index (AI) while *Matsui et al.* [2004] observed a similar correlation between AI and column-mean cloud effective radius but note that this effect is strongly modulated by atmospheric stability. These results suggest that cloud lifetime may be increased and the probability of precipitation-size droplets within a cloud decreased in the presence of enhanced CCN concentrations.

[4] Further evidence for the suppression of rainfall by aerosols is provided by the study of *Berg et al.* [2006] who show that differences in rainfall estimates from the Tropical Rainfall Measuring Mission (TRMM) Microwave Imager (TMI) and Precipitation Radar (PR) in the East China Sea can exceed 50% in the winter season because of the frequent occurrence of high LWP clouds that go undetected by the PR. Detailed analysis of a case study from this region using MODIS, CloudSat, and TRMM products in combination with idealized model simulations suggest that these clouds may owe their origins to enhanced concentrations of sulfate aerosols in the region that tend to increase the amount of cloud water required for the onset of precipitation [*Berg et al.*, 2008]. On the basis of statistical analysis of 16 months of satellite data, *Lebsock et al.* [2008] confirmed that the LWP of precipitating clouds tends to be increased in the presence of aerosols although their results also suggest that aerosols lead to a decrease in the LWP of nonprecipitating clouds, highlighting the importance of considering precipitation processes when studying aerosol indirect effects. The current study seeks to expand upon these findings by using a combination of multisensor satellite cloud and precipitation products and aerosol information from both satellite observations and a global transport model to assess the sensitivity of precipitation in warm clouds to increased aerosol concentrations.

[5] It has also been suggested that larger aerosol particles such as dust and sea salt, may serve as giant CCN (GCCN) that can enhance the development of precipitation in some clouds [*Johnson*, 1982; *Feingold et al.*, 1999; *van den Heever et al.*, 2006]. Despite having been alluded to as early as the work of *Houghton* [1938], direct observational evidence for the effects of GCCN on precipitation is somewhat limited ranging from evidence of enhanced rainfall downstream of paper mills in Washington and South Africa [e.g., *Eagan et al.*, 1974; *Hindman et al.*, 1977a, 1977b; *Mather*, 1991] to evidence that large CCN can immediately act as embryonic raindrops inducing precipitation in cumulus clouds off the coast of Florida [*Laird et al.*, 2000]. *Rosenfeld et al.* [2002] provided one of the few studies employing satellite data to investigate the effects of GCCN on precipitation over oceanic regions. On the basis of two case studies they conclude that the presence of sea-salt-generated embryonic raindrops enhances the rate at which sulfate particles are washed out of the atmosphere leading to a progressive reduction in the suppression of precipitation by pollution with increasing distance from the coast. GCCN may, therefore, play an important role in off-setting the effects of increasing CCN concentrations although it has generally been difficult to establish evidence for this effect on the global scale [*Jones and Slingo*, 1997]. Toward the goal of demonstrating and ultimately quantifying the global effects of GCCN on the incidence of rainfall in warm clouds, the current study further attempts to segregate and contrast the effects of CCN and GCCN on global precipitation occurrence using aerosol species information from a global transport model.

[6] This paper employs a unique combination of multisensor satellite data sets, numerical weather prediction (NWP) output, and aerosol distributions from both satellite observations and a global transport model to isolate and quantify the impacts of aerosols on the onset of precipitation in warm clouds. Precise delineation of raining areas from CloudSat are used to establish the probability of precipitation (POP) as a function of Advanced Microwave Scanning Radiometer (AMSR-E) liquid water path in the context of different aerosol regimes defined both through satellite products and a global transport model. The primary goals of this study are to provide a direct assessment of the impact of aerosols on the depth and microphysical properties of precipitating clouds, assess the sensitivity of precipitation to aerosols as a function their LWP and the thermodynamic properties of the environment, and qualitatively contrast the effects of CCN and GCCN on precipitation occurrence. Among the challenges of using satellite aerosol products is their lack of availability in cloudy and raining scenes, their inability to isolate concentrations of different species within a single pixel, and the potential impacts of three-dimensional cloud effects on the interpretation of aerosol signatures [*Wen et al.*, 2007]. These deficiencies can be partially addressed by using aerosol distributions from global transport models that yield a more globally continuous data set and can provide insights into the dominant aerosol species in any region [e.g., *Kawamoto et al.*, 2006; *Avey et al.*, 2007]. In addition, potential biases introduced by the scavenging of aerosols by precipitation are largely mitigated by using model-derived aerosol fields since parameterized rainfall in the model only crudely represents the real-world distribution and intensity of precipitation. On the other hand, uncertainties in the parameterizations of aerosol sources and sinks in the transport model can lead to errors in predicted aerosol concentrations. In this study we assess the sensitivity of precipitation incidence in warm clouds to aerosols using both satellite and model-derived aerosol products in an effort to overcome the weaknesses of each source individually. Consistency between parallel analyses employing observed and model-derived aerosol fields provides a more compelling case for a causal relationship between aerosols and the formation of precipitation in warm clouds.

2. Data Sets

2.1. Satellite Products

[7] The precise discrimination of raining and nonraining scenes that is central to this study is provided by the CloudSat level 2C-PRECIP-COLUMN product that is based on the algorithm of *Haynes et al.* [2009]. Despite the effects of attenuation in heavier rainfall, the excellent

sensitivity of CloudSat's Cloud Profiling Radar (CPR) (~ -30 dBZ) coupled with it's small ($\sim$1.5 km) field of view (FOV) make it ideally suited for detecting rainfall [*Ellis et al.*, 2009]. CPR radar reflectivity measurements near the ocean surface, when corrected for attenuation, provide a direct measure of drop size that can be linked to the likelihood of surface rainfall. To account for attenuation, the path integrated attenuation (PIA) is estimated from difference between the measured normalized backscatter coefficient of the surface and that expected in clear-sky conditions which can be predicted using surface wind speed and sea surface temperature. PIA is then used to correct the observed reflectivity in the lowest clutter-free range gate above the surface (typically 600–840 m) for the attenuation caused by cloud and rain above it. Higher values of unattenuated radar reflectivity in this range gate are associated with increased likelihood of precipitation and values greater than 0 dBZ are assumed to be indicative of the presence of rainfall at the surface. Wherever rain is detected, the algorithm uses Monte Carlo simulations of the relationship between attenuation and rain rate to make an of estimate rainfall intensity that explicitly accounts for the effects of snow, mixed-phase hydrometeors in the melting layer, and multiple scattering.

[8] Cloud and aerosol information is gleaned from coincident estimates of liquid water path (LWP) at 12 km resolution from the Advanced Microwave Scanning Radiometer (AMSR-E) Level 2B Global Swath Ocean Product [*Wentz*, 1997; *Meissner and Wentz*, 2002] and co-located aerosol optical depth (AOD) and Angstrom exponent from the Moderate Resolution Imaging Spectroradiometer (MODIS) Level 3 Daily One-degree Aerosol Product (Collection 5) [*Platnick et al.*, 2003]. This combination of microwave, visible, and infrared radiances combined with active cloud radar reflectivity, all of which fly now in formation as part of the A-Train, represent the first time the necessary sensors have been co-located allowing the direct assessment of the way that aerosols modify precipitation on the global scale. Rather than aggregating these data to a common grid, differences in spatial resolution and imperfect co-location of these products (MODIS aerosol data, for example, are only available in clear regions adjacent to clouds) are accommodated by employing statistical analysis of global data sets from the entire 2007 calendar year such that grid mismatches and spatial co-location errors become essentially random uncertainties. It should be noted, however, that with the exception of CloudSat data, only column-integrated products are used in this study so explicit co-location in the vertical is not possible.

[9] Using the CloudSat cloud mask product 2B-GEOPROF, the data are further restricted to clouds that are shallower than the freezing level from European Centre for Medium Range Weather Forecasts (ECMWF) to isolate systems where precipitation development is dominated by coalescence processes. Furthermore, very shallow drizzle that is completely obscured by ground clutter will not be detected by CloudSat and is, therefore, also excluded from enter the analysis. Finally, it should be noted that it is often not possible to precisely determine the base of warm clouds using CloudSat observations because of a combination of ground-clutter effects and an inability to distinguish rain from cloud in the observed reflectivities. This has implications for the analysis of cloud thickness in section 5 but it will be argued that cloud base is likely less susceptible to aerosol influences than cloud top.

2.2. Model Data

[10] On the basis of the work of *Matsui et al.* [2004, 2006] aerosol indirect effects are strongly modulated by regional atmospheric thermodynamics. Following the lead of these studies, we delineate regions with different atmospheric stability using the lower tropospheric static stability (LTSS) defined as the difference in potential temperature between 700 mb and the surface, $\Delta\theta = T_{700}\left(\frac{p_0}{p_{700}}\right)^{R/c_p} - T_{sfc}\left(\frac{p_0}{p_{sfc}}\right)^{R/c_p}$ where p is pressure, T is temperature, R is the gas constant of air, and c_p is the specific heat capacity at a constant pressure [*Klein and Hartmann*, 1993]. In order to estimate LTSS, the satellite products are supplemented with profiles of temperature and humidity from the ECMWF analyses that have been matched to the CloudSat footprint as part of the standard CloudSat algorithm data processing stream to form part of the ECMWF-AUX product. The ECMWF-AUX Interface Control Document, available from the CloudSat Data Processing Center (http://cloudsat.cira.colostate.edu), provides a more complete description of this product.

[11] Independent aerosol information to explore the impacts of co-location errors and wet scavenging that may bias exclusively satellite-based analyses as well as to discriminate distinct chemical species is provided by the Spectral Radiation-Transport Model for Aerosol Species (SPRINTARS) global aerosol transport model. By coupling a model of aerosol sources and sinks with an atmospheric general circulation model (AGCM), SPRINTARS predicts the spatial and vertical distributions of the number and mass concentrations of five aerosol species including sulfates, sea salt, dust, organic carbon, and black carbon (see the work of *Takemura et al.* [2000, 2002, 2005] for more detail). In this study, daily estimates of column-integrated visible optical depth for each species at $\sim$1 degree spatial resolution are used in parallel with MODIS products to establish the consistency of precipitation trends between these two disparate sources of aerosol information.

3. Probability of Precipitation in Maritime Clouds

[12] The globally and annually averaged probability that CloudSat detects precipitation is plotted as a function of AMSR-E LWP in Figure 1. Figure 1 forms the basis of the statistical methodology for identifying aerosol impacts on precipitation in subsequent sections. The solid black line corresponds to the fraction of CloudSat pixels that exhibit attenuation-corrected near-surface reflectivities in excess of 0 dBZ indicating the presence of precipitation-size raindrops at this level. This curve illustrates that there is, in practice, no unique threshold LWP above which a cloud can be assumed to be raining but rather that the probability of rainfall increases monotonically through the range of LWP from $\sim$150–450 gm^{-2}. Furthermore, because of the high probability of inhomogeneity within the large AMSR-E footprint it is not possible to define LWP bounds for which one can be certain that the pixel is either not raining or

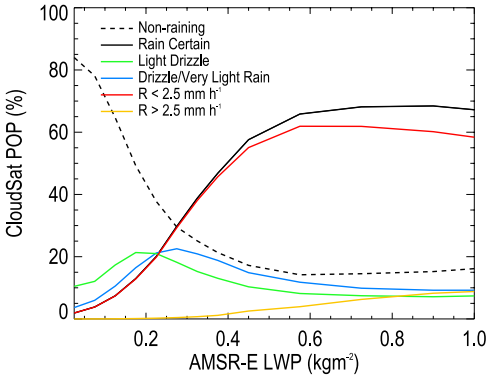

Figure 1. CloudSat probability of rainfall as a function of AMSR-E LWP (solid black curve) and its breakdown into light ($R < 2.5$ mm h^{-1}) and moderate ($R > 2.5$ mm h^{-1}) intensity ranges (red and orange curves, respectively). The dashed curve indicates the probability that the pixel is not raining or drizzling whereas the green and blue curves represent the probability of light drizzle and moderate drizzle, respectively.

definitely raining. At very low LWP there is always some nonnegligible probability that CloudSat will detect rainfall in the AMSR-E FOV and there is always some possibility of clear air within the FOV even at very high LWP (dashed curve). In fact, the asymptotic nature of the CloudSat probability of precipitation (POP) above 600 gm^{-2} suggest that, on average, any given AMSR-E FOV is only ever 70% filled with rainfall.

[13] In addition to the 0 dBZ "Rain Certain" threshold for rainfall, the CloudSat rainfall detection algorithm applies two additional thresholds of −15 dBZ and −7 dBZ to identify pixels that may contain drizzle ($R < 0.01$ mm h^{-1}) and very light rainfall ($0.01 < R < 0.03$ mm h^{-1}), respectively. These two rainfall categories are represented by the green and blue curves in Figure 1, respectively, indicating a gradual transition from extremely light drizzle at lower LWP to rainfall in wetter clouds. Similarly, the breakdown of certain rainfall into less than or greater than 2.5 mm h^{-1} (red and yellow curves, respectively) indicates a gradual transition from all light rainfall at low LWP to a progressively higher frequency of heavier precipitation at LWP above 500 gm^{-2}.

3.1. Influence of Atmospheric Thermodynamics

[14] The dominant influence governing the development of precipitation in the clouds examined here is the large-scale thermodynamic properties of the atmosphere in which they reside [*Klein*, 1997]. Using the LTSS as a proxy for atmospheric stability, CloudSat rainfall probability is plotted as a function of AMSR-E LWP for various stability ranges in Figure 2. Here, and in all plots that follow, only the "Rain Certain" category from the 2C-PRECIP-COLUMN product is considered. POP generally increases systematically with increasing stability at LWP greater than 250 gm^{-2}. This reflects the fact that precipitating clouds are likely to be more homogeneous across the AMSR-E footprint and less vertically developed in stable environments resulting in larger liquid water contents for a given LWP. Interestingly, this trend reverses itself with a distinct crossover between 200 and 250 gm^{-2}. Below this threshold the probability of CloudSat detecting rainfall within the AMSR-E FOV decreases with increasing stability. This is likely caused by isolated raining cumulus clouds that can easily be detected by CloudSat but that are much smaller than AMSR-E footprint (causing their LWP to be averaged with surrounding clear regions) that are more likely to occur in unstable environments.

[15] The slope of POP with respect to LTSS is plotted as a function of LWP in Figure 2b. Error bars represent uncertainty in each slope calculation owing to uncertainty and scatter in the CloudSat POP estimates and only slopes that are statistically significant at the 95% confidence level are reported. Since these error estimates are central to the interpretation of the results that follow, their origins are briefly discussed here. The problem of estimating POP reduces to two counting problems, one for the number of precipitating pixels and the other for the total number of samples. Such problems are governed by the Poisson distribution and their standard deviation is given by $\sqrt{N}$ where N is the total number of counts [*Taylor*, 1997]. Defining POP as $P = \frac{N_r}{N_t}$ where N_r and N_t are the number of raining and total number of CloudSat pixels, respectively, the uncertainty in POP can be determined from standard error propagation

$$\delta P = \sqrt{\left(\frac{\partial P}{\partial N_r}\right)^2 (\delta N_r)^2 + \left(\frac{\partial P}{\partial N_t}\right)^2 (\delta N_t)^2} \tag{1}$$

$$= P\sqrt{\frac{1}{N_r} + \frac{1}{N_t}} \tag{2}$$

This result assumes that all CloudSat observations are independent but, since adjacent CloudSat footprints are separated by less than 1 km, much shorter than the spatial scale of typical precipitation events, the CloudSat observations are autocorrelated along the satellite ground track.

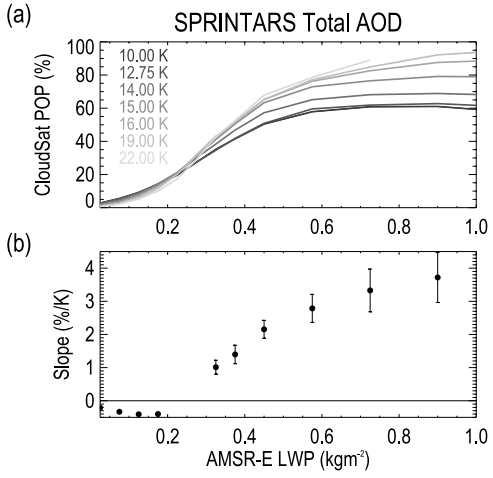

Figure 2. Probability of precipitation as a function of LWP for various LTSS defined using ECMWF analyses. The bottom presents the slope of POP with respect to LTSS for those values of LWP where it is statistically significant at the 95% level.

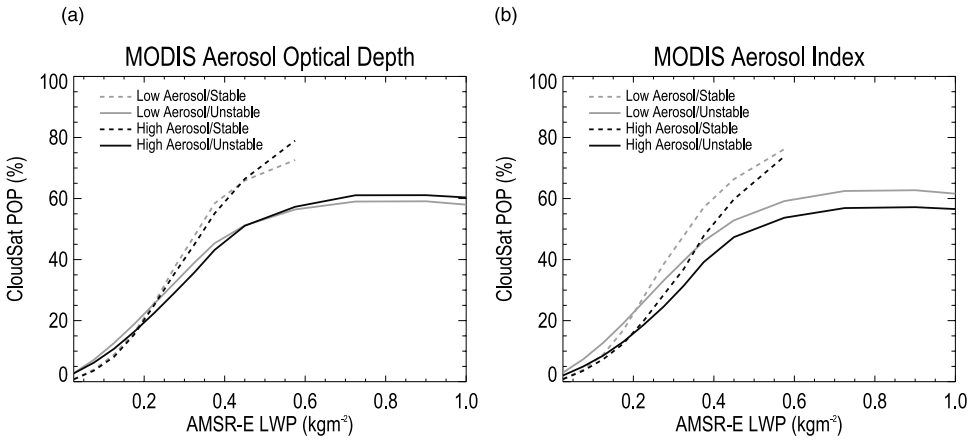

Figure 3. As in Figure 2 but data are now stratified by both LTSS and (a) MODIS aerosol optical depth and (b) MODIS aerosol index.

Autocorrelations are accounted for by reducing N_r and N_t to better represent the effective number of degrees of freedom in the data set

$$N' = \frac{N}{1 + \sum_{k=1}^{N-1}\left(1 - \frac{k}{N}\right)\rho(k)} \tag{3}$$

where $\rho(k) = \frac{1}{\sigma^2}Cov(x_i, x_{i+k})$ is the autocorrelation function determined by spatially correlating the PIA measurements for all precipitating pixels in the CloudSat data set. These estimates of uncertainty in POP and effective number of degrees of freedom in each data subset subsequently used in standard approaches for assessing statistical significance in all results presented below. In Figure 2b and throughout the remainder of the manuscript, only slopes that are statistically significant at the 95% confidence level are reported. It is important to note, however, that there is always a possibility for systematic biases in satellite products as a function of the local environment because of their complex dependence on assumptions that are often buried deep within the algorithms used to generate them [*Berg et al.*, 2006]. Identifying and quantifying such biases is a topic of ongoing research and, as a result, they are not addressed by the estimates of statistical significance presented here.

3.2. Influence of Aerosols

[16] To assess the impacts of aerosols on the initiation of rainfall in warm maritime clouds, the POP-LWP analysis is repeated with data stratified by both LTSS and various proxies for aerosol concentration. Figure 3 compares POP-LWP relationships between stable and unstable environments and those with high and low aerosol concentrations from MODIS observations. Results are stratified by both MODIS AOD and aerosol index (AI) that is defined as the product of optical depth and the Angstrom exponent that more completely closely relates to aerosol number concentration [*Nakajima et al.*, 2001]. Stable and unstable environments are defined by LTSS greater than 18 K and less than 13.5 K, respectively, representing the most and least stable 10% of the data set. The definitions of high and low aerosol concentrations are summarized in Table 1. Figure 4 repeats the analysis for each of the five different species of aerosol reported by SPRINTARS as well as the total SPRINTARS aerosol optical depth. In all cases the ranges of values used to define the high and low aerosol categories have been chosen to ensure that the sample sizes in each category were approximately consistent although it should be noted that because of variations in the geographic distribution of each species it is not possible to ensure that the sampling remains constant across all LWP bins.

[17] Figure 3 suggests that CloudSat POP tends to exhibit a distinct trend with MODIS AI where the rainfall probability for any given LWP tends to decrease in the presence of enhanced AI in both stable and unstable environments. Equivalently, the results suggest that higher LWPs are required for precipitation to develop in regions of high aerosol index. Since AI has been shown to be representative of the column concentration of CCN [*Nakajima et al.*, 2001], this result reflects a suppression of precipitation in the presence of higher concentrations of small aerosol particles. In stable environments this effect is largest at lower water paths in the range 200–350 gm^{-2} while the POP sensitivity to aerosol index is spread over higher LWP in unstable regions. Interestingly, there is little evidence for a similar trend when MODIS AOD is used to stratify the data. This emphasizes the importance of small aerosol that serve as CCN over other forms of aerosol that also impact AOD.

[18] Additional insights into the different roles of large and small aerosol particles are provided in Figure 4 where the aerosol signature is broken down by chemical species provided by SPRINTARS. Sulfate aerosols, that are typically small and contribute significantly to measured aerosol

Table 1. Definitions of Low and High Aerosol Categories for Each MODIS Variable and SPRINTARS Species Shown in Figures 3 and 4

Variable	Low Aerosol	High Aerosol
MODIS optical depth	0.0–0.08	0.16–0.5
MODIS aerosol index	0.0–0.5	0.15–1.0
SPRINTARS sulfate	0.0–0.008	0.03–0.5
SPRINTARS sea salt	0.0–0.05	0.082–0.4
SPRINTARS organic carbon	0.0–0.0012	0.02–0.2
SPRINTARS black carbon	0.0–0.0004	0.0035–0.02
SPRINTARS dust	0.0–0.0012	0.006–0.2
SPRINTARS total	0.0–0.018	0.055–0.5

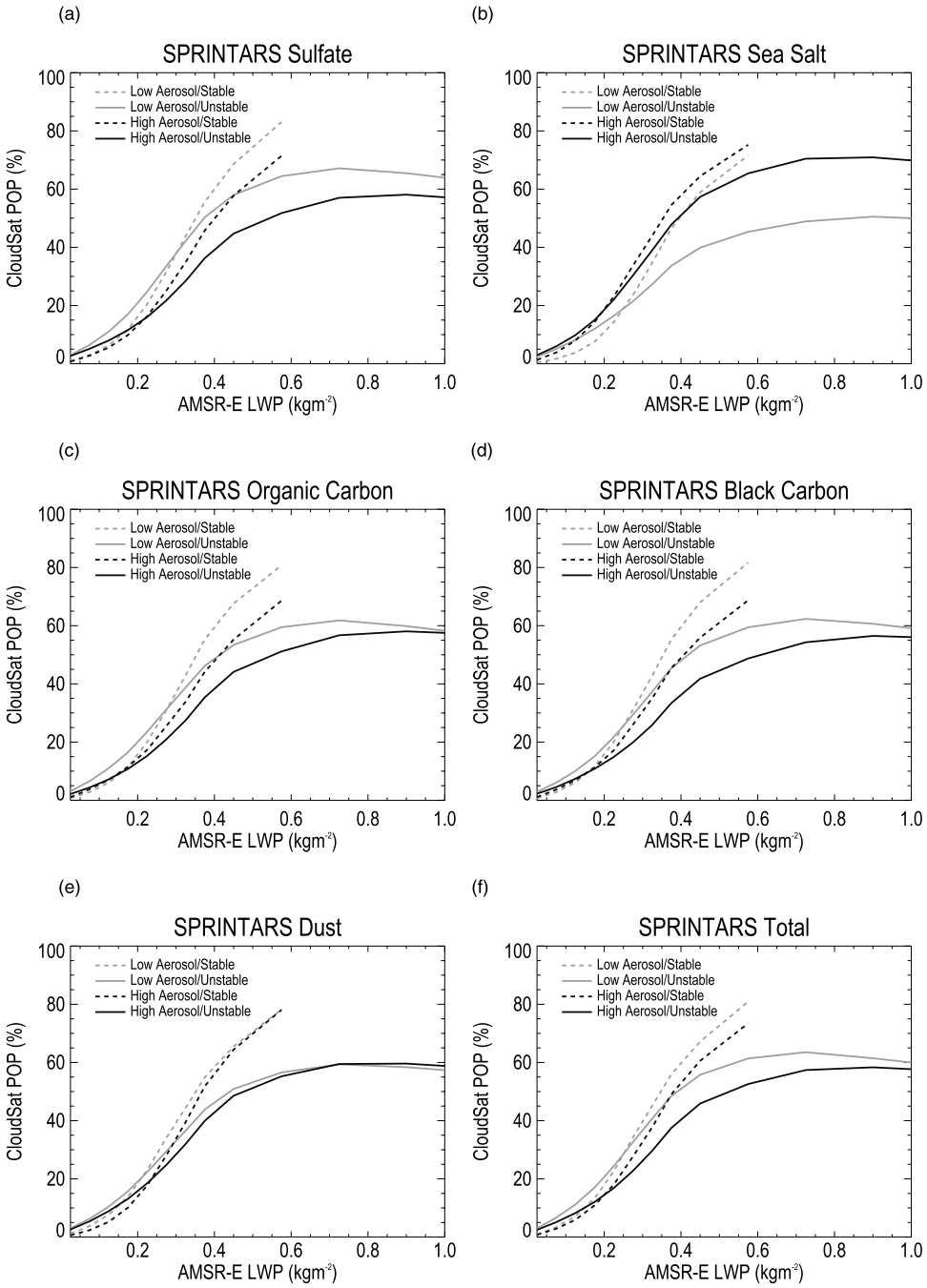

Figure 4. As in Figure 3 but for SPRINTARS aerosol optical depths: (a) sulfate, (b) sea salt, (c) black carbon, (d) organic carbon, (e) dust, and (f) total.

index, exhibit a signature that very closely resembles that of the MODIS AI. This is a significant result given the disparate nature of the sources of aerosol information being used and confirms the findings of *Chameides et al.* [2002] who found consistency in trends in cloud optical depth derived using independent aerosol information from a regional transport model and the International Satellite Cloud Climatology Project (ISCCP). Similarities in the dependence of POP on MODIS AI and SPRINTARS sulfate AOD not only ease sampling concerns associated with the fact that satellite aerosol observations must be interpolated into cloudy regions from adjacent clear areas but also establish confidence in the use of transport models for gaining deeper insights into the role of distinct species of aerosols. Perhaps the most significant benefit of using both observed and model-derived aerosol properties in this analysis lies in strengthening the case for causality. It can, for instance, be argued that the strictly observational analysis of MODIS, AMSR-E, and CloudSat data are not sufficient for establishing the role of aerosols as driving the observed suppression of precipitation. Instead, one could argue that it is possible that aerosols are more effectively scavenged in environments with more frequent precipitation leading to an anticorrelation between aerosol

Table 2. Global Correlations Between Various SPRINTARS Aerosol Species Over the Period From January to December 2007

	Total	Sulfate	Sea Salt	Dust	Organic Carbon	Black Carbon
Total	1.0	0.53	−0.12	0.88	0.51	0.52
Sulfate	0.53	1.0	−0.03	0.11	0.61	0.53
Sea salt	−0.12	−0.03	1.0	−0.10	−0.11	−0.16
Dust	0.88	0.11	−0.10	1.0	0.10	0.19
Organic carbon	0.51	0.61	−0.11	0.10	1.0	0.83
Black carbon	0.52	0.53	−0.16	0.19	0.83	1.0

index and POP that is entirely independent of aerosol impacts on microphysics. The fact that a very similar relationship exists between model-based SPRINTARS sulfate aerosol and POP, however, supports the argument that it is the aerosols themselves that suppress the precipitation and not the other way around since there is no direct pathway for observed changes in precipitation efficiency to modify model-derived aerosol fields.

[19] Figure 4b provides evidence that sea-salt aerosols may exert an opposite influence on warm clouds than sulfates. In unstable environments there is a clear trend toward increased POP in regions of high sea-salt concentrations and this trend tends to increase with increasing LWP. A possible explanation for this may lie in fact that sea-salt aerosols are typically much larger (>1 μm) than sulfates and when these particles are activated they likely form larger embryonic raindrops rather than the smaller cloud particles that tend to form on sulfate CCN [*Laird et al.*, 2000]. Thus instead of inhibiting the coalescence

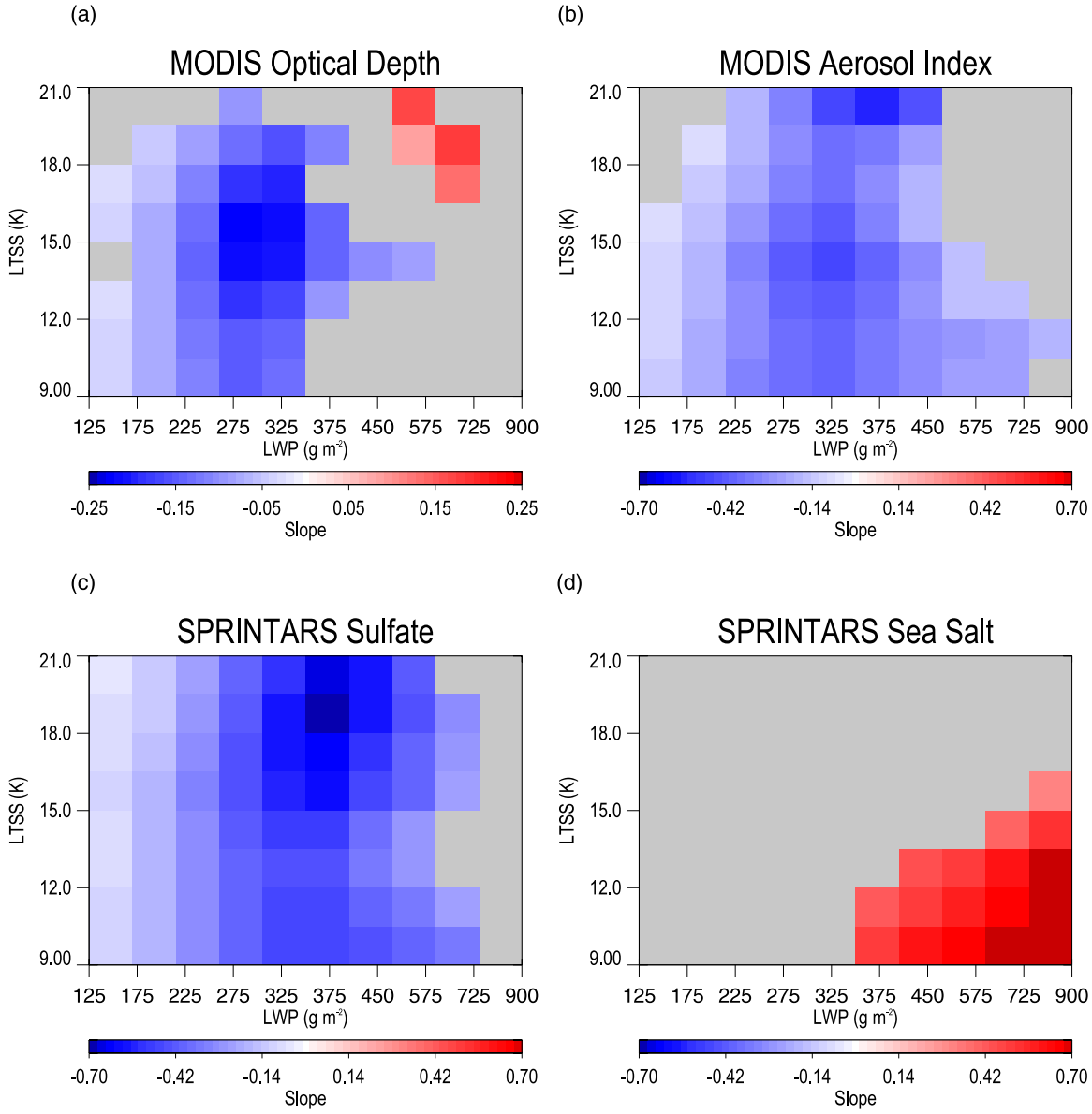

Figure 5. Slope of POP versus AOD for different combinations of LTSS and LWP. The top corresponds to (a) MODIS optical depth and (b) aerosol index, respectively. The bottom corresponds to (c) SPRINTARS sulfate and (d) SPRINTARS sea-salt aerosols. Gray regions represent slopes that are not statistically significant at the 95% confidence level.

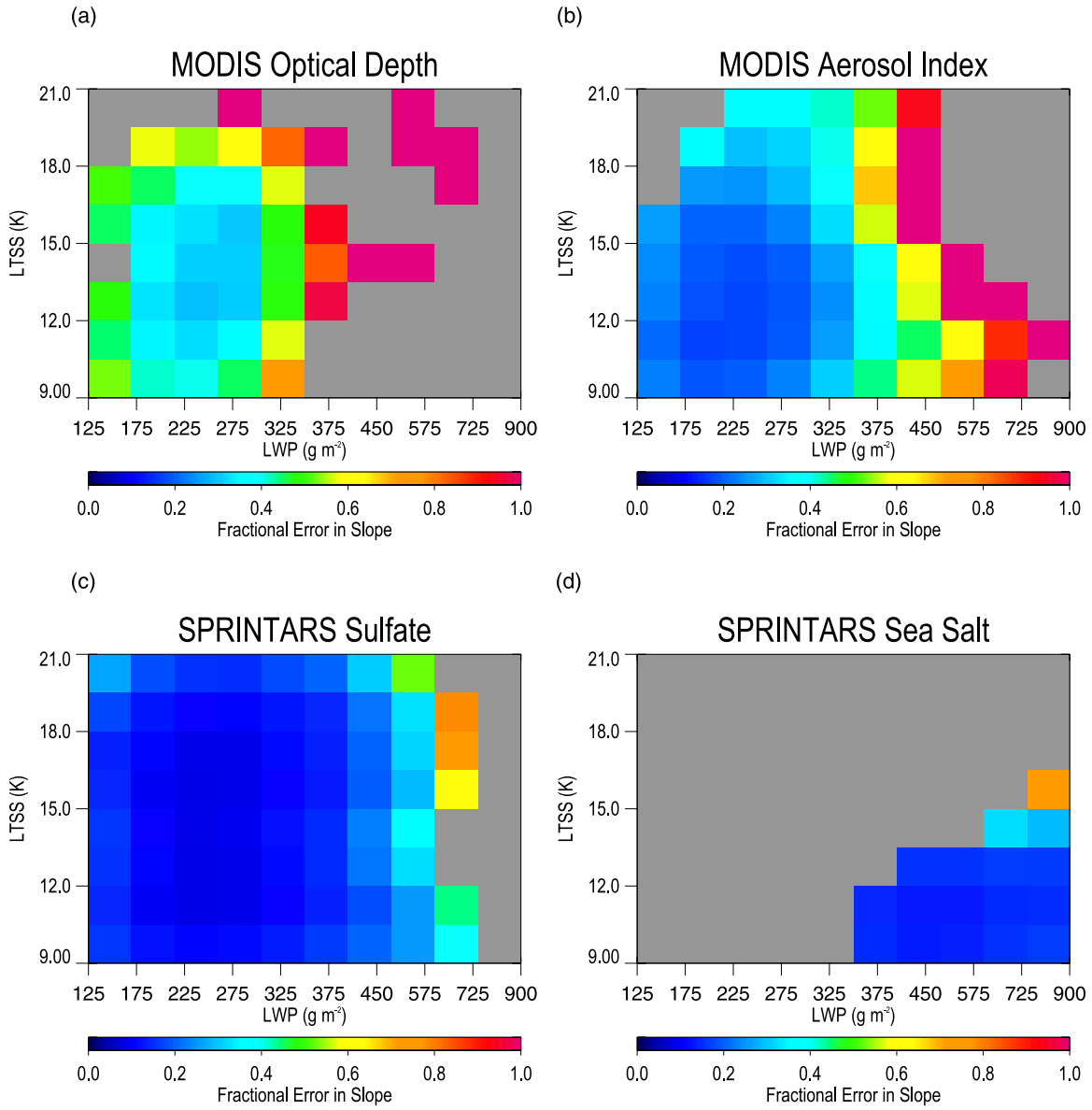

Figure 6. Fractional uncertainties in the slopes represented in Figure 5.

process like sulfates, sea-salt aerosols accelerate the broadening of cloud drop spectra required to initiate precipitation processes in clouds for a given LWP. Similar arguments have been made by previous studies to suggest that sea salts may reduce the effectiveness of anthropogenic sulfate aerosols over oceans [e.g., *Jones and Slingo*, 1997; *Rosenfeld et al.*, 2002] but unlike these studies the results presented here suggest that sea salt may actually increase precipitation incidence in warm clouds. This effect could dominate the effects of anthropogenic aerosols in regions of strong surface winds where larger concentrations of sea-salt aerosols may enhance the precipitation efficiency of local clouds. In addition, the lack of a clear aerosol signature in Figure 3 may now be attributed to a combination of the competing effects of sulfate and sea-salt aerosols that cannot be separated using satellite-derived AOD information alone. In fact, there is evidence of a transition in the precipitation sensitivity to MODIS AOD from a reduction in POP at low LWP to an increase at high LWP that is consistent with the regions of LWP where sulfates and sea-salt effects are greatest. These trends are not, however, statistically significant by the definition provided in section 3.

[20] Similar trends in probability of precipitation exist when data are stratified by SPRINTARS organic and black carbon (Figures 4c and 4d). However, it must be pointed out that regions of high organic and black carbon tend to be strongly correlated with high sulfate concentrations (Table 2) making it impossible to distinguish the effects of these different species. Given the hygroscopic nature of sulfate aerosols and their larger concentrations in general, it is likely that the some of the observed trends with carbonaceous aerosols can be attributed to the effects of sulfates but the results hint at the possibility that these species may also act to suppress precipitation. On the basis of Table 1, sea-salt aerosols are generally uncorrelated with sulfates allow-

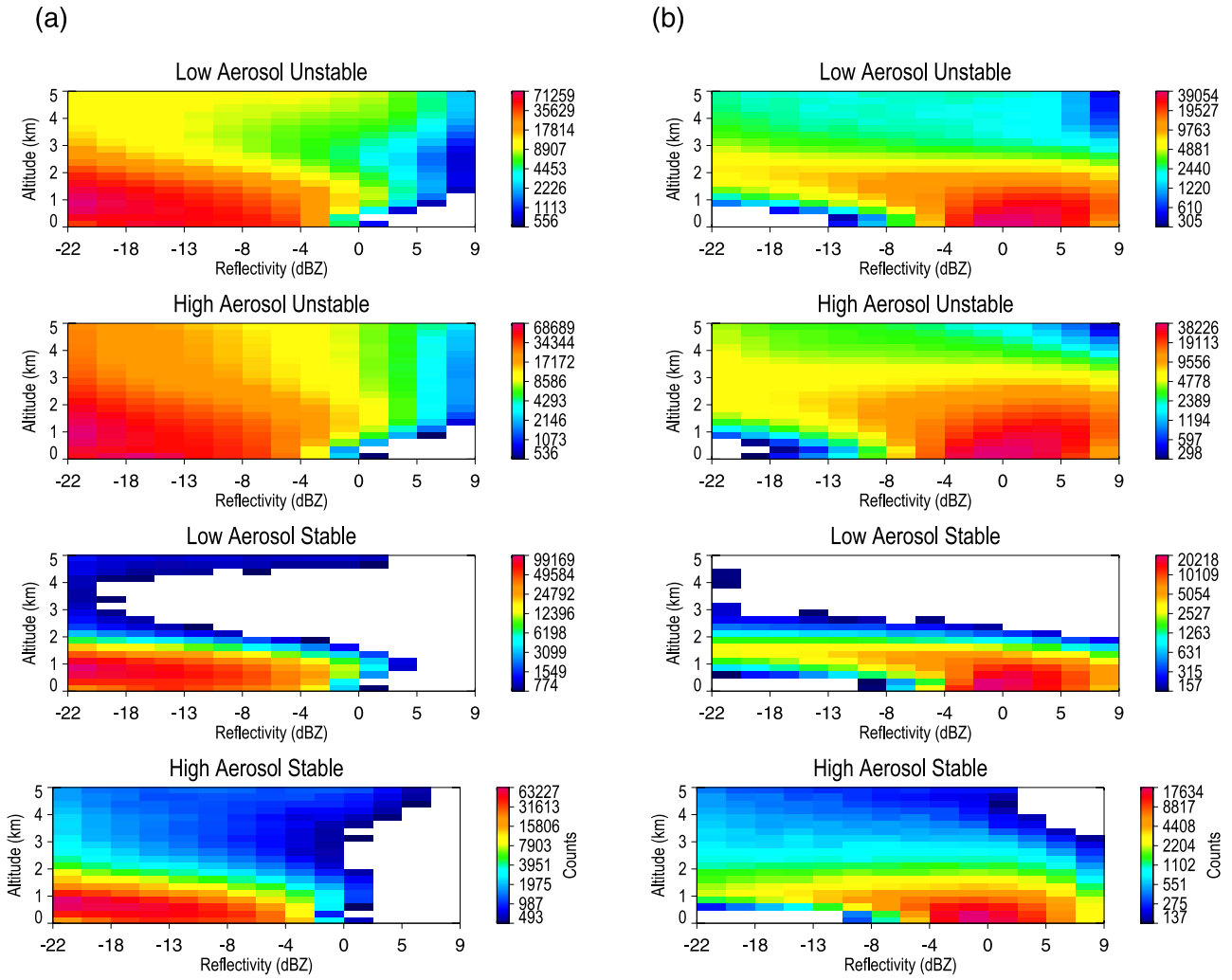

Figure 7. Reflectivity-altitude histograms (RAHs) of CloudSat observed reflectivities for (a) nonraining and (b) raining pixels. The top corresponds to unstable conditions with low concentrations of sulfate aerosols whereas the remaining represent high sulfate concentration; unstable, low sulfate concentration; stable, and high sulfate concentration; and stable conditions, respectively.

ing these species to be analyzed separately with a high degree of confidence. Dust is not well correlated with either sea salt or sulfate but also fails to generate a clear impact on the probability of rainfall in the warm clouds examined here. As a result the analysis that follows will be restricted to exploring the apparently competing effects of sea-salt and sulfate aerosols on precipitation in more detail.

4. Regime Dependence

[21] From Figure 4 there is evidence that the influence of aerosols on precipitation incidence depends on cloud LWP and atmospheric thermodynamics, that we refer to collectively as the "cloud regime". Sulfate aerosols, for example, appear to have the largest impact on clouds with intermediate LWP in unstable environments. Sea-salt impacts, on the other hand, are maximum at high LWP but also exhibit a markedly larger signature in unstable environments. To more completely assess the impact of aerosols in different cloud regimes the slope of POP with respect to observed and model-derived aerosol properties is summarized for a wide range of LWP and stability combinations in Figure 5. The sensitivity of changes in POP to sulfates (Figure 5c) shows that the trend toward reduced probability of precipitation with increasing sulfate AOD holds for most stability and LWP bins. The magnitude of this effect, however, depends strongly on the type of cloud and thermodynamic properties of its environment. Decreases in POP are weak in low liquid water path clouds, for example, since precipitation is very rare in such scenes regardless of ambient aerosol concentrations. Similarly, the presence of higher CCN concentrations has little impact on high LWP clouds where cloud water is plentiful enough that enormous concentrations of CCN would be required to significantly impact the coalescence process. Clouds with water paths between 250 and 375 gm^{-2} are, therefore, most sensitive to increases in sulfate AOD. Furthermore, since clouds in this LWP range are more likely to precipitate in stable environments, the suppression effects of sulfate aerosols tend to be somewhat larger at high LTSS.

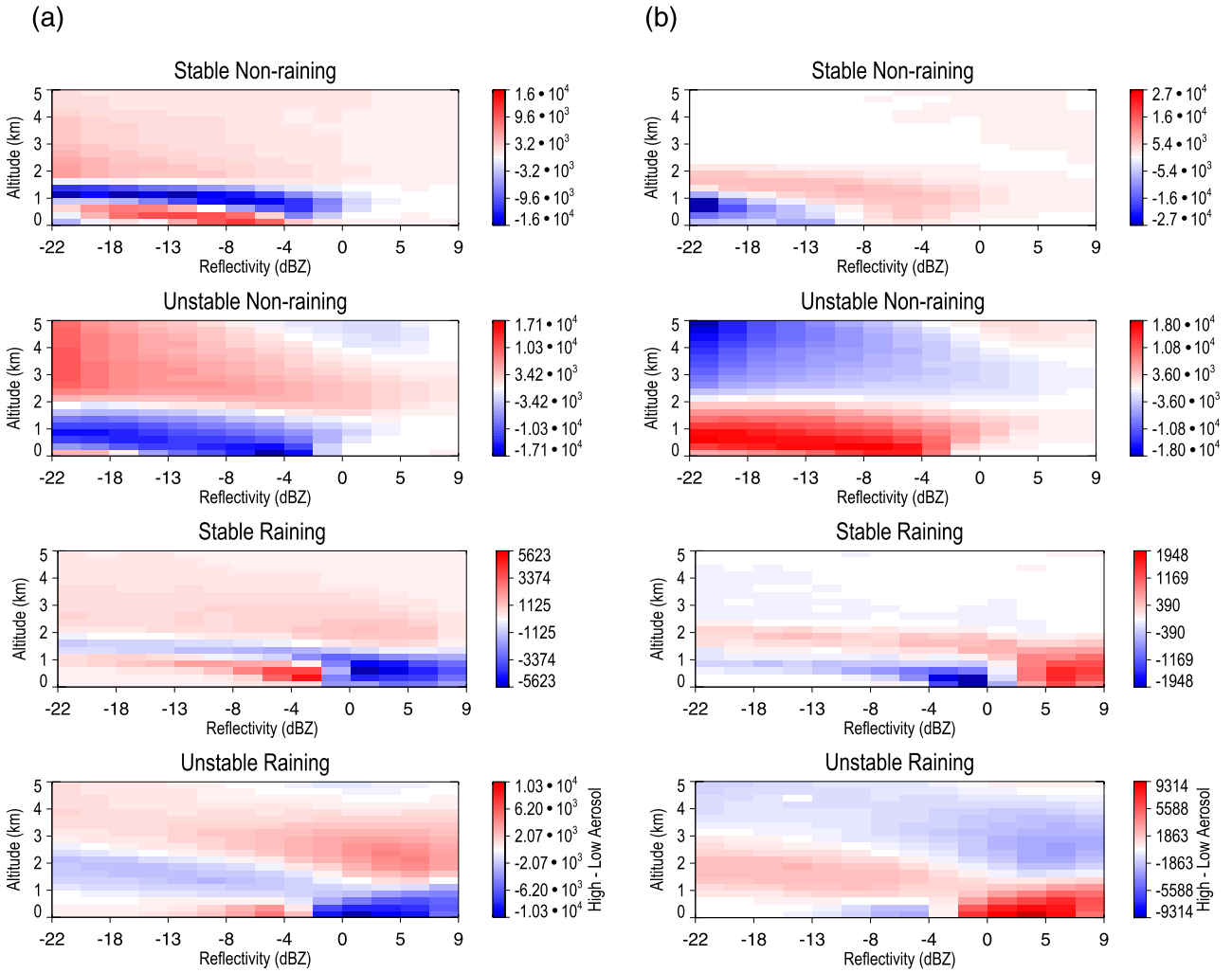

Figure 8. Differences between RAHs in environments with (a) high and low sulfate aerosol concentrations and (b) high and low sea-salt aerosol concentrations. Nonraining stable and unstable conditions are shown in the top whereas the raining stable and unstable conditions are shown in the bottom.

[22] Differences in the sensitivity of POP to sulfates and sea salts (Figure 5d) is striking. POP increases systematically with increasing sea-salt AOD although in this case rainfall probability is enhanced most effectively at high LWP and in unstable environments. This suggests that sea-salt particles accelerate the development of rainfall in "wet" clouds and, in particular, those that reside in unstable regions. One possible explanation for this result is the more rapid formation of embryonic raindrops on sea-salt nuclei that subsequently grow rapidly by collecting the abundant cloud droplets consistent with the modeling studies of *Feingold et al.* [1999] and *Lu and Seinfeld* [2005].

[23] Figure 5 also reinforces the notion that MODIS AI generally represents the impacts of sulfate aerosols although the magnitudes of the trends in POP with MODIS AI are somewhat smaller, possibly because of our inability to obtain satellite aerosol concentrations in the immediate vicinity of clouds and precipitation. For high LWP clouds in unstable environments, the competing effects of sea salt and sulfates that cannot be distinguished using AOD alone reduce sensitivities with respect to MODIS AOD to levels that are no longer statistical significant. This offers a potential explanation for the observation of *Bréon et al.* [2002] that cloud droplet size is better correlated with AI than AOD but also suggests that exclusively using AI to study the aerosol impacts may underrepresent the important competing effect of much larger sea-salt particles.

[24] Fractional uncertainties in the slope of POP with respect to aerosol are presented in Figure 6. In addition to the test of statistical significance that has been applied to mask slopes that are not significant at the 95% confidence level, the fact that fractional uncertainties in slope calculations are often less than 20% in the analysis of SPRINTARS data reinforces the fact that the relationships between POP and aerosol are robust. Slopes of POP with respect to MODIS AI tend to be a factor of two less certain than those with respect to SPRINTARS data, possibly indicative of the effects of cloud-aerosol co-location errors or wet scavenging that impact satellite aerosol observations. Finally, trends with respect to MODIS AOD are significantly less certain than any other source of aerosol information consistent with the fact that AOD alone cannot adequately distinguish the

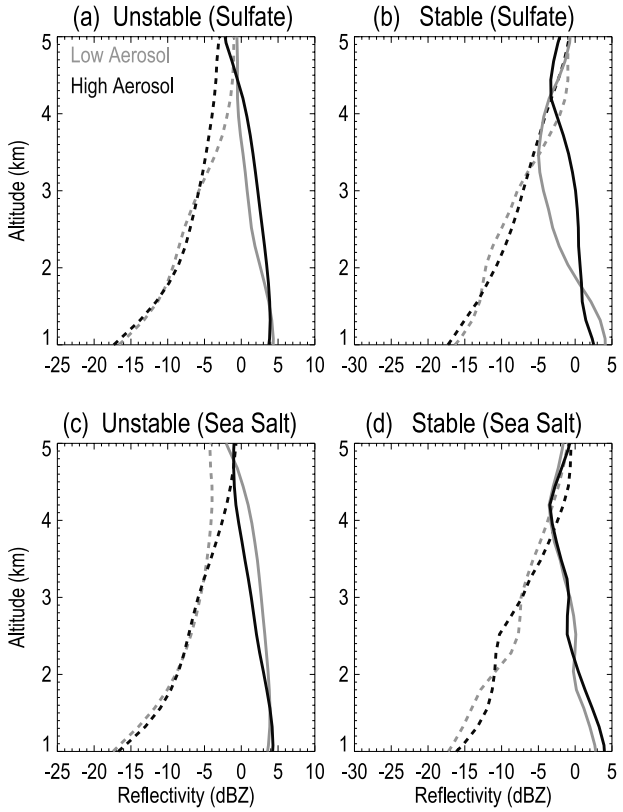

Figure 9. Average vertical profiles of radar reflectivity for the scenes depicted in Figure 8. The top corresponds to sulfate aerosols whereas the bottom is for sea salt. Dashed curves correspond to nonprecipitating clouds whereas solid curves represent precipitating clouds.

competing effects of small and large aerosols over a large range of LWP and LTSS.

5. Implications for Cloud Vertical Development

[25] It has been suggested that modifying the onset of precipitation in warm clouds may have significant impacts on their evolution and microphysical properties. It may, therefore, be anticipated that the observed modification of the onset of precipitation by aerosols might also manifest itself through corresponding changes in cloud drop size, cloud lifetime, and cloud vertical development. Several previous studies have explored the impact of aerosols on cloud lifetime and particle size by relating satellite measurements of cloud extent, water path, and effective radius to observations of aerosols in adjacent clear areas [e.g., *Bréon et al.*, 2002; *Sekiguchi et al.*, 2003; *Lebsock et al.*, 2008]. Here a different approach is adopted that is rooted in the statistical analysis of CloudSat reflectivity profiles segregated by ancillary aerosol products.

[26] Although the infrequent sampling characteristic of polar orbiting satellites makes it difficult to directly monitor the evolution of individual clouds, these satellites ultimately sample all phases of the life cycle of all cloud regimes over time. This "composite" view of cloud structure obtained by accumulating vast numbers of snapshots of different cloud systems at different stages in their life cycle can provide some insights into the manner by which aerosols impact cloud morphology in a global sense. Figure 7, for example, shows histograms of CloudSat radar reflectivity as a function of height for raining and nonraining pixels under different environmental conditions. These reflectivity-altitude histograms (RAHs) provide a means of condensing millions of snapshots of individual cloud systems into a single mean reflectivity structure, that is representative of the complete lifecycle of average clouds in the given environment. Changes in the rate at which clouds evolve from one phase of their development to another manifest themselves as changes in the relative frequency of occurrence of that structure in the RAH. For example, there is a distinct tendency for both precipitating and nonprecipitating clouds to grow deeper in unstable environments evidenced by the higher concentration of reflectivity values at higher altitudes in the unstable RAHs. There is also a clear shift in reflectivity from lower values in nonprecipitating clouds to higher values in precipitating clouds indicating the presence of much larger droplets in the latter.

[27] The effects of aerosol are more subtle and more difficult to discern in Figure 7 although there is some evidence of clouds growing deeper in the higher aerosol environment. To highlight these differences more clearly, differences between RAHs observed in high and low aerosol environments are presented in Figure 8. Regions in reflectivity-height space that are enhanced in the presence of higher aerosol concentrations appear in red while blue areas denote reflectivity-height values that decrease in frequency in response to aerosols. The impacts of sulfate aerosols are highlighted in Figure 8a. The trend toward deeper clouds, particularly in unstable environments, can be inferred from the distinct increase in the frequency of reflectivities at higher altitudes at the expense those at lower levels. In addition, there is a clear shift in lower level reflectivity in raining pixels from higher values to lower values indicated by the blue region around 5 dBZ and the corresponding red region around −4 dBZ in Figure 8a (bottom). Since reflectivity varies as the 6th power of drop size, this is evidence of a decrease in the size of raindrops in the presence of enhanced sulfate aerosol concentrations. While the link between RAHs and cloud lifetime is tenuous at best, Figure 8 provides consistent evidence that sulfate aerosol may inhibit precipitation. The results imply that the enhanced CCN concentrations in the high sulfate aerosol case suppress the broadening of the drop size spectrum that is normally associated with the formation of drizzle in warm clouds resulting in deeper clouds before the onset of precipitation, particularly in unstable environments. This is consistent with the findings of *Koren et al.* [2005] who suggested that delaying the onset of warm rain may result in stronger local updrafts caused by additional latent heat release prior to the development of offsetting downdrafts associated with precipitation. It is reasonable to expect this effect to be more pronounced in unstable environments where cloud height is not strongly capped by large-scale thermodynamics.

[28] The change in cloud structure caused by enhanced concentrations of sea-salt aerosols is summarized in Figure 8b exhibiting almost a reciprocal image of the impact of sulfate aerosols. Clouds in unstable environments tend to be significantly less vertically developed in the presence of

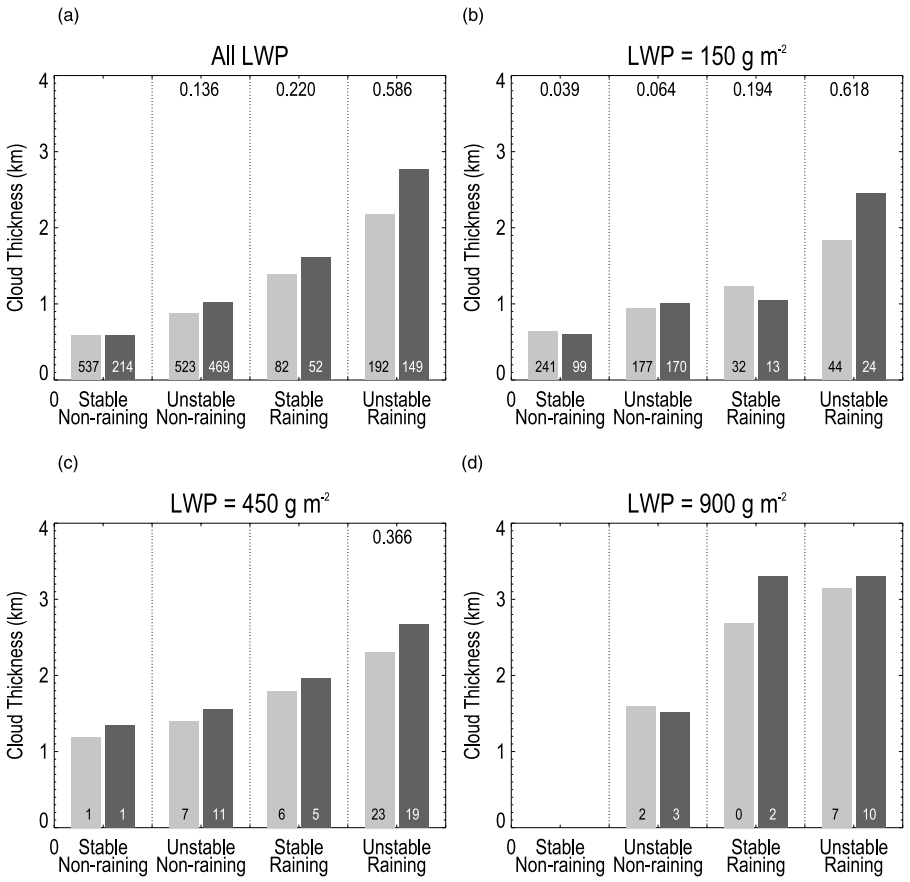

Figure 10. Impacts of sulfate aerosols on cloud vertical development for the four environments defined in Figure 3. Low and high sulfate aerosol concentrations are represented by light and dark gray bars, respectively. The number of samples in each category (in thousands) is reported at the base of each bar. The magnitude of the difference in cloud height between low and high aerosol environments is summarized above each pair of bars whenever it is statistically significant at the 95% confidence level.

sea-salt aerosols and there is a distinct shift toward larger rain drops in precipitating clouds. This further supports the assertion that the activation of sea-salt particles accelerates the broadening of the cloud drop spectrum allowing coalescence to begin more quickly. Clouds in sea-salt-rich environments, therefore, may precipitate more quickly reducing the available water content, stabilizing the local environment, and failing to grow as deep in initially unstable environments.

[29] To better isolate the impacts of aerosols on the mean drop size of clouds in different environments, conditional mean vertical profiles of reflectivity for each environment are presented in Figure 9. These results more clearly demonstrate the significant increase in reflectivity aloft and an equivalent reduction in reflectivity at lower levels in the presence of enhanced concentrations of sulfate aerosols and indicate that, while cloud depth tends to increase, raindrop size tends to be reduced in polluted environments. Sea-salt aerosols again exhibit an inverse signature but in this case the decreases in cloud depth are more pronounced in unstable environments while increases in raindrop size are most pronounced in stable environments.

[30] The influence of sulfate aerosols on cloud depth is further isolated and quantified in Figure 10. Since it is often difficult to determine cloud base from CloudSat because of ground clutter (and impossible in raining pixels where reflectivities extend down to the surface), cloud base is assumed to extend to the lowest range bin where CloudSat sees an unambiguous cloud signal. While this may introduce uncertainty in estimates of cloud thickness, it is assumed that the impact of aerosols on cloud base height is much smaller than their effect on cloud top since the former is dictated by atmospheric thermodynamics while the latter is also sensitive to cloud lifetime. Under this assumption, cloud base errors will exhibit the same statistical behavior in both polluted and clean environments effectively canceling from the perspective of discussing relative differences between them. Figure 10 indicates that clouds are typically deeper in sulfate-rich environments. The effect is particularly pronounced for precipitating clouds in unstable environments that tend to be $\sim$600 m deeper in regions with high sulfate concentrations.

[31] Figures 10b–10d indicate that the magnitude of the impact of sulfate aerosols on cloud depth also depends on LWP. The largest increases in cloud depth are observed lower LWPs and are no longer statistically significant at the

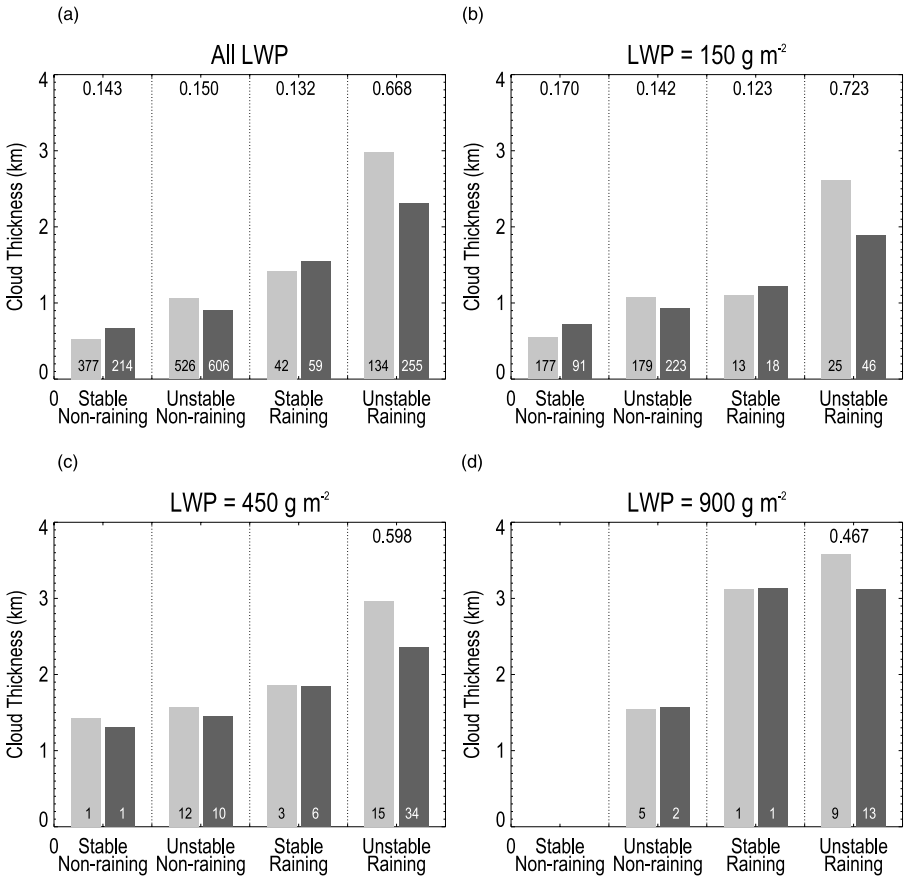

Figure 11. As in Figure 10 but for SPRINTARS sea-salt aerosols.

highest LWP considered. This is indicative of a "saturation" effect where the clouds with the highest water paths have already grown to the maximum height allowed, i.e., the freezing level, and cannot be further deepened by the presence of aerosols because of the warm cloud constraint imposed on this analysis.

[32] Equivalent results for sea-salt aerosols are presented in Figure 11 again illustrating a trend opposite to that introduced by sulfates. The largest impacts of sea salts are also for precipitating clouds in unstable environments but in this case statistically significant reductions in cloud height extend to all LWP thresholds. This supports the assertion that the mechanism by which sea salts influence marine clouds is through an accelerated initial broadening of the cloud droplet distribution leading to the generation of embryonic raindrops and reduced local updrafts that inhibit further vertical development of these clouds by the reciprocal argument to that made by *Koren et al.* [2005].

6. Conclusions

[33] The analysis of multisensor satellite products from Aqua and CloudSat in the context of both observed and model-derived aerosol fields yields a number of consistent pieces of evidence for the suppression of precipitation by sulfate aerosols on a global scale. Clouds in polluted environments tend to exhibit smaller mean drop sizes, have lower probabilities of rainfall for a given LWP, and grow deeper than their counterparts in more pristine environments. The results also provide the first direct global evidence for the competing effect of large sea-salt aerosols that tend to enhance precipitation formation in a manner that is consistent with previous regional studies. When combined with additional evidence that precipitating clouds in such environments tend to be less vertically developed and contain larger raindrops, these results suggest that the nucleation of sea-salt particles may systematically enhance the broadening of the cloud drop size distribution in maritime clouds causing precipitation to form at lower liquid water contents and ultimately reducing cloud lifetime.

[34] The distinction between sulfate and sea-salt impacts relies heavily on the ability of SPRINTARS to provide realistic distributions of the global distributions of distinct aerosol species, an assertion that is difficult to test. The credibility of the results is, however, strengthened by the smooth and systematic variation of the deduced trends across all stability and water path bins. Consistency between trends in particle size, cloud depth, and precipitation incidence that are each derived from distinct sources further reduces the likelihood that the observed trends are merely artifacts of modeling uncertainties. The primary findings are also found to be qualitatively similar to those obtained using independent aerosol information from MODIS. Trends in cloud properties with respect to MODIS data indicate that the number concentration of CCN is more closely related to the product of optical depth and Angstrom exponent while

AOD alone represents both changes in the number and size of the aerosols present. Thus the effects of CCN and GCCN on precipitation occurrence tend to offset one another in analyses with respect to AOD while AI tends to isolate CCN impacts.

[35] While it is not possible to completely isolate the impacts of different aerosol species because of correlations between their locations and modeling errors, the uniform relationships that emerge from analyzing satellite observations in the context of independent model-derived aerosol fields suggest that the impact of aerosols on warm rain occurrence could be either positive or negative depending on the species involved. The competing nature of these processes is likely to have important implications for estimating the overall impact of aerosols on global precipitation since the net change in POP in any region will depend strongly on the relative frequency of types of clouds that are most susceptible to each aerosol species.

[36] **Acknowledgments.** This research was supported by NASA grant NNX07AR97. CloudSat data were acquired through the DPC and can be accessed through their Web site http://www.cloudsat.cira.colostate.edu. AMSR-E liquid water path data are produced by Remote Sensing Systems and sponsored, in part, by NASA's Earth Science Information Partnerships (ESIP): a federation of information sites for Earth science; and by the NOAA/NASA Pathfinder Program for early EOS products; principal investigator: Frank Wentz. MODIS aerosol products were obtained from the Goddard Distributed Active Archive Center (DAAC).

References

Albrecht, B. (1989), Aerosols, cloud microphysics, and fractional cloudiness, *Science*, *245*, 1227–1230.

Avey, L., T. J. Garrett, and A. Stohl (2007), Evaluation of the aerosol indirect effect using satellite, tracer transport model, and aircraft data from the International Consortium for Atmospheric Research on Transport and Transformation, *J. Geophys. Res.*, *112*, D10S33, doi:10.1029/2006JD007581.

Berg, W., T. L'Ecuyer, and C. Kummerow (2006), Rainfall climate regimes: The relationship of regional TRMM rainfall biases to the environment, *J. Appl. Meteorol. Climatol.*, *45*, 434–454.

Berg, W., T. L'Ecuyer, and S. van den Heever (2008), Evidence for the impact of aerosols on the onset and microphysical properties of rainfall from a combination of satellite observations and cloud resolving model simulations, *J. Geophys. Res.*, *113*, D14S23, doi:10.1029/2007JD009649.

Bréon, F.-M., D. Tanre, and S. Generoso (2002), Aerosol effect of cloud droplet size monitored from satellite, *Science*, *295*, 834–838.

Chameides, W. L., C. Luo, R. Saylor, D. Streets, Y. Huang, M. Bergin, and F. Giorgi (2002), Correlation between model-calculated anthropogenic aerosols and satellite-derived cloud optical depths: Indication of indirect effect?, *J. Geophys. Res.*, *107*(D10), 4085, doi:10.1029/2000JD000208.

Eagan, R. C., P. V. Hobbs, and L. F. Radke (1974), Particle emissions from a large Kraft paper mill and their effects on the microstructure of warm clouds, *J. Appl. Meteorol.*, *13*, 535–552.

Ellis, T., T. S. L'Ecuyer, J. M. Haynes, and G. L. Stephens (2009), How often does it rain over the global oceans? The perspective from CloudSat, *Geophys. Res. Lett.*, *36*, L03815, doi:10.1029/2008GL036728.

Feingold, G., W. R. Cotton, S. M. Kreidenweis, and J. T. Davis (1999), The impact of giant cloud condensation nuclei on drizzle formation in stratocumulus: Implications for cloud radiative properties, *J. Atmos. Sci.*, *56*, 4100–4117.

Feingold, G., W. L. Eberhard, D. E. Veron, and M. Previdi (2003), First measurements of the Twomey indirect effect using ground-based remote sensors, *Geophys. Res. Lett.*, *30*(6), 1287, doi:10.1029/2002GL016633.

Ferek, R. J., et al. (2000), Drizzle suppression in ship tracks, *J. Atmos. Sci.*, *57*, 2765–2778.

Forster, P., et al. (2007), Changes in atmospheric constituents and radiative forcing, in *Climate Change 2007: The Physical Basis. Contribution of Working Group I to the Fourth Assessment Report of the Intergovernmental Panel on Climate Change*, edited by S. Solomon et al., 996 pp., Cambridge Univ. Press, Cambridge, U. K.

Ghan, S., R. Easter, J. Hudson, and F.-M. Bréon (2001), Evaluation of aerosol indirect radiative forcing in MIRAGE, *J. Geophys. Res.*, *106*, 5317–5334.

Givati, A., and D. Rosenfeld (2004), Quantifying precipitation suppression due to air pollution, *J. Appl. Meteorol.*, *43*, 1038–1056.

Haynes, J. M., T. S. L'Ecuyer, G. L. Stephens, S. D. Miller, C. M. Mitrescu, N. B. Wood, and S. Tanelli (2009), Rainfall retrieval over the ocean using spaceborne high-frequency cloud radar, *J. Geophys. Res.*, *113*, D00A22, doi:10.1029/2008JD009973.

Hindman, E. E., II, P. V. Hobbs, and L. F. Radke (1977a), Cloud condensation nuclei from a paper mill. Part I: Measured effects on clouds, *J. Appl. Meteorol.*, *16*, 745–752.

Hindman, E. E., II, P. M. Tag, B. A. Silverman, and P. V. Hobbs (1977b), Cloud condensation nuclei from a paper mill. Part II: Calculated effects on rainfall, *J. Appl. Meteorol.*, *16*, 753–755.

Houghton, H. G. (1938), Problems connected with the condensation and precipitation processes in the atmosphere, *Bull. Am. Meteorol. Soc.*, *19*, 152–159.

Jacobson, M. Z., Y. J. Kaufman, and Y. Rudich (2007), Examining feedbacks of aerosols to urban climate with a model that treats 3-D clouds with aerosol inclusions, *J. Geophys. Res.*, *112*, D24205, doi:10.1029/2007JD008922.

Jiang, H., G. Feingold, and W. R. Cotton (2002), Simulations of aerosol-cloud-dynamical feedbacks resulting from entrainment of aerosol into the marine boundary layer during the Atlantic Stratocumulus Transition Experiment, *J. Geophys. Res.*, *107*(D24), 4813, doi:10.1029/2001JD001502.

Johnson, D. B. (1982), The role of giant and ultragiant aerosol particles in warm rain initiation, *J. Atmos. Sci.*, *39*, 448–460.

Jones, A., and A. Slingo (1997), Climate model studies of sulphate aerosols and clouds, *Philos. Trans. R. Soc. London Ser. B*, *352*, 221–229.

Jones, A., D. L. Roberts, M. J. Woodage, and C. E. Johnson (2001), Indirect sulphate aerosol forcing in a climate model with an interactive sulphur cycle, *J. Geophys. Res.*, *106*, 20,293–20,310.

Kawamoto, K., T. Hayasaka, I. Uno, and T. Ohara (2006), A correlative study on the relationship between modeled anthropogenic aerosol concentration and satellite-observed cloud properties over east Asia, *J. Geophys. Res.*, *111*, D19201, doi:10.1029/2005JD006919.

Klein, S. A. (1997), Synoptic variability of low-cloud properties and meteorological parameters in the subtropical trade wind boundary layer, *J. Clim.*, *10*, 2018–2039.

Klein, S. A., and D. L. Hartmann (1993), The seasonal cycle of low stratiform clouds, *J. Atmos. Sci.*, *6*, 1587–1606.

Koren, I., Y. J. Kaufman, D. Rosenfeld, L. A. Remer, and Y. Rudich (2005), Aerosol invigoration and restructuring of Atlantic convective clouds, *Geophys. Res. Lett.*, *32*, L14828, doi:10.1029/2005GL023187.

Laird, N. F., H. T. Ochs III, R. M. Rauber, and L. J. Miller (2000), Initial precipitation formation in warm Florida cumulus, *J. Atmos. Sci.*, *57*, 3740–3751.

L'Ecuyer, T. S., N. B. Wood, T. Haladay, G. L. Stephens, and P. W. Stackhouse (2008), The impact of clouds on atmospheric heating based on the R04 CloudSat fluxes and heating rates data set, *J. Geophys. Res.*, *113*, D00A15, doi:10.1029/2008JD009951.

Lebsock, M., G. L. Stephens, and C. Kummerow (2008), Multisensor observations of aerosol effects on warm clouds, *J. Geophys. Res.*, *113*, D15205, doi:10.1029/2008JD009876.

Lohmann, U., and J. Feichter (2001), Can the direct and semi-direct aerosol effect compete with the indirect effect on a global scale?, *Geophys. Res. Lett.*, *28*, 159–161.

Lu, M.-L., and J. H. Seinfeld (2005), Study of the aerosol indirect effect by large-eddy simulation of marine stratocumulus, *J. Atmos. Sci.*, *62*, 3909–3932.

Mather, G. K. (1991), Coalescence enhancement in large multicell storms caused by the emissions from a Kraft paper mill, *J. Appl. Meteorol.*, *30*, 1134–1146.

Matsui, T., H. Masunaga, R. A. Pielki Sr., and W.-K. Tao (2004), Impact of aerosols and atmospheric thermodynamics on cloud properties within the climate system, *Geophys. Res. Lett.*, *31*, L06109, doi:10.1029/2003GL019287.

Matsui, T., H. Masunaga, S. M. Kreidenweis, R. A. Pielki Sr., W.-K. Tao, M. Chin, and Y. Kaufman (2006), Satellite-based assessment of marine low cloud variability associated with aerosol, atmospheric stability, and the diurnal cycle, *J. Geophys. Res.*, *111*, D17204, doi:10.1029/2005JD006097.

Meissner, T., and F. J. Wentz (2002), Analysis of the ocean surface wind direction signal in passive microwave brightness temperatures, *IEEE Trans. Geosci. Remote Sens.*, *40*, 1230–1240.

Nakajima, T., A. Higurashi, K. Kawamoto, and J. E. Penner (2001), A possible correlation between satellite-derived cloud and aerosol microphysical parameters, *Geophys. Res. Lett.*, *28*, 1171–1174.

Platnick, S., M. D. King, S. A. Ackerman, W. P. Menzel, B. A. Baum, J. C. Riedi, and R. A. Frey (2003), The MODIS cloud products: Algorithms

and examples from Terra, *IEEE Trans. Geosci. Remote Sens.*, *41*, 459–473.
Rosenfeld, D. (2000), Suppression of rain and snow by urban and industrial air pollution, *Science*, *287*, 1793–1796.
Rosenfeld, D., et al. (2002), The role of sea spray in cleansing air pollution over the ocean via cloud processes, *Science*, *297*, 1667–1670.
Rotstayn, L. D., and Y. Liu (1999), Sensitivity of the first indirect aerosol effect to an increase of droplet spectral dispersion with droplet number concentration, *J. Clim.*, *16*, 3476–3481.
Sekiguchi, M., T. Nakajima, K. Suzuki, K. Kawamoto, A. Higurashi, D. Rosenfeld, I. Sano, and S. Mukai (2003), A study of the direct and indirect effects of aerosols using global satellite data sets of aerosol and cloud parameters, *J. Geophys. Res.*, *108*(D22), 4699, doi:10.1029/2002JD003359.
Squires, P. (1956), The microstructure of cumuli in maritime and continental air, *Tellus*, *8*, 443–444.
Squires, P. (1958), The microstructure and colloidal stability of warm clouds. Part I: The relation between structure and stability, *Tellus*, *10*, 256–261.
Takemura, T., H. Okamoto, Y. Maruyama, A. Numaguti, A. Higurashi, and T. Nakajima (2000), Global three-dimensional simulation of aerosol optical thickness distribution of various origins, *J. Geophys. Res.*, *105*, 17,853–17,873.
Takemura, T., T. Nakajima, O. Dubovik, B. N. Holben, and S. Kinne (2002), Single-scattering albedo and radiative forcing of various aerosol species with a global three-dimensional model, *J. Clim.*, *15*, 333–352.
Takemura, T., T. Nozawa, S. Emori, T. Y. Nakajima, and T. Nakajima (2005), Simulation of climate response to aerosol direct and indirect effects with aerosol transport-radiation model, *J. Geophys. Res.*, *110*, D02202, doi:10.1029/2004JD005029.
Taylor, J. R. (1997), *An Introduction to Error Analysis*, 2nd ed., 327 pp., Univ. Science Books, Suasalito, Calif.
Twomey, S. (1977), The influence of pollution on the shortwave albedo of clouds, *J. Atmos. Sci.*, *34*, 1149–1152.
Twomey, S., M. Piepgrass, and T. L. Wolfe (1984), An assessment of the impact of pollution on global cloud albedo, *Tellus*, *36B*, 356–366.
van den Heever, S. C., G. G. Carrio, W. R. Cotton, P. J. DeMott, and A. J. Prenni (2006), Impacts of nucleating aerosol on Florida storms. Part I: Mesoscale simulations, *J. Atmos. Sci.*, *63*, 1752–1774.
Wen, G., A. Marshak, R. F. Cahalan, L. A. Remer, and R. G. Kleidman (2007), 3-D aerosol-cloud radiative interaction observed in collocated MODIS and ASTER images of cumulus cloud fields, *J. Geophys. Res.*, *112*, D13204, doi:10.1029/2006JD008267.
Wentz, F. J. (1997), A well-calibrated ocean algorithm for SSM/I, *J. Geophys. Res.*, *102*, 8703–8718.

W. Berg, J. Haynes, M. Lebsock, and T. S. L'Ecuyer, Department of Atmospheric Science, Colorado State University, Fort Collins, CO 80523, USA. (tristan@atmos.colostate.edu)

T. Takemura, Research Institute for Applied Mechanics, Kyushu University, 6-1 Kasuga-koen, Kasuga, Fukuoka 816-8580, Japan.